Applied and Computational Mechanics 5 (2011) 151–162

Car impact to pedestrian – fast 2D numerical analysis

L. Hynčík[a,*], H. Čechová[a]

[a] *New Technologies – Research Centre, University of West Bohemia, Univerzitní 8, 306 14 Plzeň, Czech Republic*

Received 9 March 2011; received in revised form 20 September 2011

Abstract

The paper concerns a modelling approach for fast 2D car to pedestrian impact analysis. The pedestrian model is composed using the Lagrange equations with multipliers. The model consists of rigid bodies defining the major human body segments. The bodies are connected by rotational joints with non-linear response. The model is scalable based on the age and the gender. The car model is multi-segment composed as an open polygon. Between the pedestrian and the car, there are contacts defined and modelled explicitly by force-penetration dependence. For a given car profile design and a given human gender, age and percentile, the pedestrian impact consequences can be evaluated quickly by means of virtual numerical analysis.

Keywords: contact, pedestrian, impact, multi-body numerical simulation

1. Introduction

The traffic accidents are within a group of external consequences causing the third highest number of death in the Czech Republic, just after deaths caused by falls and suicides [15]. The numbers of deaths or fatally injured citizens prove that the traffic accidents and their consequences are still a serious problem to be solved. The statistics show that the number of accidents decreases slowly in the past years [14]. However, the decrease is necessary to be speed up regarding also the socioeconomic aspects of the problem [4].

2. Motivation

A lot of effort is devoted to both passive and active safety systems development where virtual human body models start to play significant role since they become powerful tool for supporting development of human-friendly and safe vehicles by the numerical way using computer simulation. Regarding that the correct biofidelic models are necessary to be developed and validated [7]. However such complete models usually spend a lot of computational time. Having a set of structural designs of a vehicle to be analysed, simple models are usually sufficient tool for the first approximation. Based on the standard injury criteria implemented in the simple models, they might predict global human behaviour and injuries in very short computational time. Hence, a lot of structural designs and impact scenarios might be analysed quickly in order to choose the best one for a deeper analysis.

3. Method

The paper shows the numerical modelling approach towards pedestrian impact analysis. Currently, two-dimensional (2D) modelling approach is presented.

*Corresponding author. Tel.: +420 377 634 709, e-mail: hyncik@ntc.zcu.cz.

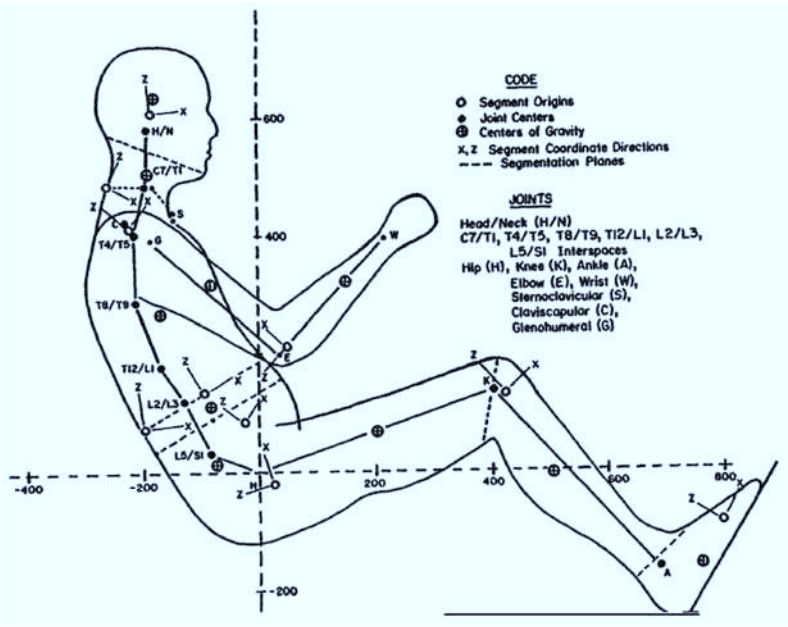

Fig. 1. Human body segmentation (taken from [12])

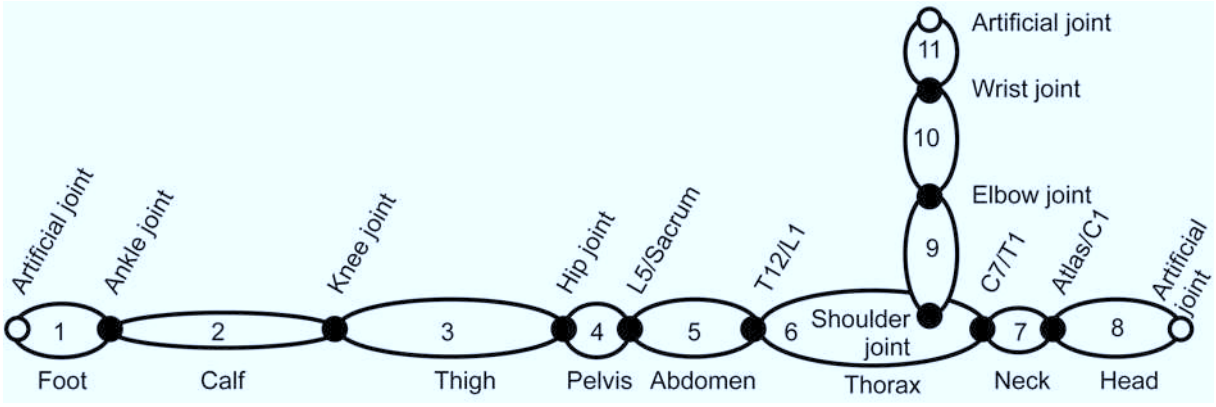

Fig. 2. Human body open-tree multi-body system in the horizontal position

3.1. Geometry and segmentation

The basic human body segmentation is taken from Robbins [12], see Fig. 1. The segmentation is as simple as possible to ensures the full articulability and correct kinematics of the human body under the loading. The anthropometry defined in Robbins [12] also presents the 50 %-tile male body including mass distribution, moments of inertia evaluation and joint stiffness definiton.

Based on the above-mentioned segmentation, the human body model is structured as a linked open-tree multi-body system (see Fig. 2) implemented using the Lagrange's equations with multipliers. The model is composed by 11 segments Ω_i, $i \in \{1, \ldots, 11\}$. The segments correspond to 11 rigid bodies, namely:

- Head
- Neck
- Thorax
- Abdomen
- Pelvis
- Left and right arm
- Left and right forearm
- Left and right hand
- Left and right thigh
- Left and right calf
- Left and right foot

Due to the planar (2D) approach, the couple segments (arm, forearm, hand, thigh, calf and foot) are considered as a one single segment.

3.2. Mass distribuion and joints

The position of each segment is geometrically defined by the centre S_i, $i \in \{1, \ldots, 11\}$ located between 2 joints $\boldsymbol{K}_{i,i-1}$ and $\boldsymbol{K}_{i,i+1}$ connecting the segment to the previous and the following segment in the tree system. The exception is for the head, the hand and the foot that are the outer segments. In this case, an artificial joint supplying the missing second joint is defined for the segment length measuring purposes. The segment centre

$$\boldsymbol{S}_i = \frac{\boldsymbol{K}_{i,i-1} + \boldsymbol{K}_{i,i+1}}{2} \tag{1}$$

is an origin of the particular segment local coordinate system. The first local coordinate system axis is defined as

$$\bar{\boldsymbol{e}}_1 = \frac{\boldsymbol{K}_{i,i+1} - \boldsymbol{S}_i}{\|\boldsymbol{K}_{i,i+1} - \boldsymbol{S}_i\|} \tag{2}$$

and the second one $\bar{\boldsymbol{e}}_2$ is a unit vector perpendicular $\bar{\boldsymbol{e}}_1$ constructing a clock-wise system. Each segment carries its mass m_i and moment of inertia I_i, $i \in \{1, \ldots, 11\}$ concentrated to its centre of gravity $T_i = \left[{}^T\bar{x}_i, {}^T\bar{y}_i\right]$, $i \in \{1, \ldots, 11\}$ where the bar denotes coordinates in the segment local coordinate system $(\bar{\boldsymbol{e}}_1, \bar{\boldsymbol{e}}_2)$. The scheme is shown in Fig. 3.

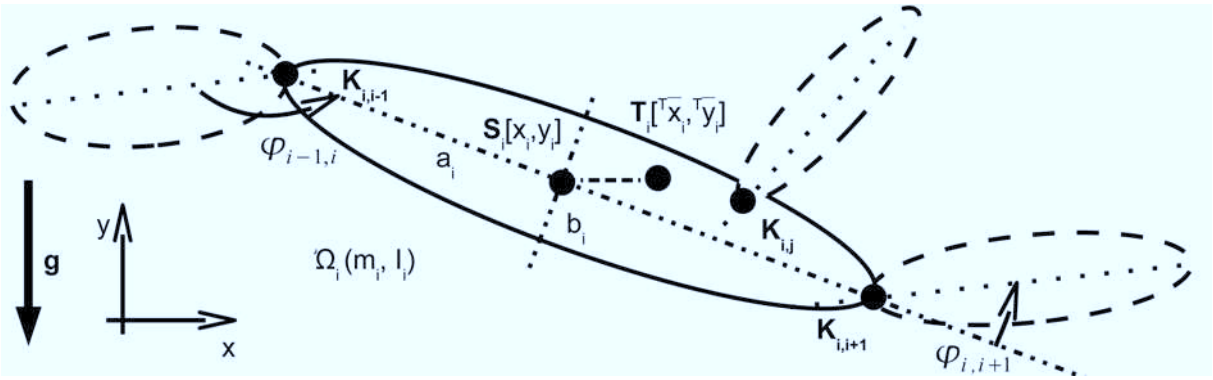

Fig. 3. Segment definition

Two neighbouring segments are connected by joints. The full model accommodates 10 joints, namely:

- Head/neck joint in the position between vertebrae Atlas bone and C1
- Neck/thorax in the position between vertebrae C7 and T1
- Thorax/abdomen in the position between vertebrae T12 and L1
- Abdomen/pelvis in the position between vertebrae L5 and Sacrum bone
- Left and right shoulder
- Left and right elbow
- Left and right wrist
- Left and right hip
- Left and right knee
- Left and right ankle

With respect to the Robbins segmentation [12], all joints in the current model are modelled as rotational ones accommodating non-linear rotational stiffness. Due to the planar approach, the couple joints (shoulder, elbow, wrist, hip knee and ankle) are concentrated into one single joint having double stiffness.

3.3. Anthropometry and stiffness scaling

The basic 50 %-tile human body anthropometry and mass distribution is based on [12] (for both male and female). The details of the scaling can be found in [8]. Due to the simple modelling approach and no detailed segment shape description, only the height based scaling is concerned. Bláha [2] defines the height from ground of all the above-mentioned joints in the human upright standing position, so the particular segment height can be obtained by substraction. The data measured by Bláha [2] depends on gender and age from 0 till 75 years.

Let us define a length vector $\boldsymbol{l}_i = \boldsymbol{K}_{i,i+1} - \boldsymbol{K}_{i,i-1}$ for each segment Ω_i, $i \in \{1, \ldots, 11\}$. Concerning the size, each segment can be defined by its length $2a_i = \|\boldsymbol{l}_i\|$ as the distance between the joints connecting the segment to the previous and the following segment in the tree system. Considering the upright standing position of the model, each segment height can be defined as $h_i = \boldsymbol{l}_i \boldsymbol{e}_2$ in the global coordinate system $(\boldsymbol{e}_1, \boldsymbol{e}_2)$. The upright standing position of Robbins [12] is defined in [8].

Mathematically the anthropometry scaling means that the original size is multiplied by a scaling factor k_i defined as a ratio between the target height defined by [2] and the original height h_i of the segment in the upright standing positon. Concerning the head, the hand and the foot that are the outer segments the length is measured with help of the artificial joint defined above. In summary considering the uniform mass density distribution and the model upright standing position, the 3 basic points defining any segment (centre of gravity and both joints) can be scaled by multiplying by the scaling coeffitient k_i in the global coordinate system as $\tilde{\boldsymbol{x}} = k_i \boldsymbol{x}$. After the anthropometry scaling, all segments have to be reconnected in the joint positions. The mass and the moment of inertia of a particular segment change by changing its size. Considering the uniform mass density distribution, the mass and moment of inertia of each segment can be scaled as $\tilde{m} = k_i^3 m$ and $\tilde{I} = k_i^5 I$ [8], where $\tilde{m}$ and $\tilde{I}$ denotes the scaled values.

The segments are linked together using the rotational joints with non-linear stiffnesses defined in [12] for a 50 %-tile (average) subject. The joints flexibility also changes due to the age. The age dependent flexibility is also scaled based on so called flexindex [1]. Flexindex defines the flexibility of the whole human body by a single number (percentage to the average state) taking into account the flexibility of all major joints together [1]. The percentage is taken into account to multiply the all body joint ranges for the desired age.

3.4. Multi-body approach

Let us have the model structure described by rigid segments linked to an open-tree multi-body system as displayed in Fig. 3. The human model dynamical response due to the impact loading is investigated by the energy balance approach using the Lagrange's equations with multipliers. Let us have n segments, in our case $n = 11$, having the segment numbered by $i \in \{1, \ldots, 8\}$ from the foot through the tree system uptill the head and by $i \in \{6, 9, 10, 11\}$ from the thorax through the tree system uptill the hand. The motion of each segment Ω_i, $i \in \{1, \ldots, n\}$ is defined in plane by 3 independent coordinates where the first two defines the planar position of its centre of gravity and the third one the rotation around it. Let us define the vector

$$\boldsymbol{q} = [x_1, \ldots, x_n, y_1, \ldots, y_n, \varphi_1 \ldots, \varphi_n]^T \tag{3}$$

including 33 generalized coordinates that are dependent by $m = 2(n-1) = 20$ constraints

$$\begin{aligned}
\Phi_i &= -x_i + x_{i+1} - (a_i - \bar{x}_i)cos(\varphi_i) && (4)\\
&\quad -(a_{i+1} + \bar{x}_{i+1})cos(\varphi_{i+1}) - \bar{y}_i sin(\varphi_i) + \bar{y}_{i+1} sin(\varphi_{i+1}), && (5)\\
\Phi_{n-1+i} &= -y_i + y_{i+1} - (a_i - \bar{x}_i)sin(\varphi_i) && (6)\\
&\quad -(a_{i+1} + \bar{x}_{i+1})sin(\varphi_{i+1}) + \bar{y}_i cos(\varphi_i) - \bar{y}_{i+1} cos(\varphi_{i+1}), && (7)
\end{aligned}$$

where $\bar{x}_i$ and $\bar{y}_i$ are the coordinates of the segment centre of gravity in the local coordinate system (see Fig. 3) and $i \in \{1, \ldots, 7\}$ from the ankle over the legs and spine to the head/neck joint,

$$\begin{aligned}
\Phi_8 &= = -x_6 + x_9 - (\bar{x}_{shoulder} - \bar{x}_6)cos(\varphi_6) && (8)\\
&\quad -(a_9 + \bar{x}_9)cos(\varphi_9) - \bar{y}_6 sin(\varphi_6) + (\bar{y}_{shoulder} + \bar{y}_9)sin(\varphi_9), && (9)\\
\Phi_{18} &= = -x_6 + x_9 - (\bar{x}_{shoulder} - \bar{x}_6)sin(\varphi_6) && (10)\\
&\quad -(a_9 + \bar{x}_9)sin(\varphi_9) + (\bar{y}_6 - \bar{y}_{shoulder})cos(\varphi_6) - \bar{y}_9 cos(\varphi_9), && (11)
\end{aligned}$$

for the shoulder joint where $[\bar{x}_{shoulder}, \bar{y}_{shoulder}]^T$ are the coordinates of the shoulder joint in the thorax local coordinate system and

$$\begin{aligned}
\Phi_i &= -x_i + x_{i+1} - (a_i - \bar{x}_i)cos(\varphi_i) && (12)\\
&\quad -(a_{i+1} + \bar{x}_{i+1})cos(\varphi_{i+1}) - \bar{y}_i sin(\varphi_i) + \bar{y}_{i+1} sin(\varphi_{i+1}), && (13)\\
\Phi_{n-1+i} &= -y_i + y_{i+1} - (a_i - \bar{x}_i)sin(\varphi_i) && (14)\\
&\quad -(a_{i+1} + \bar{x}_{i+1})sin(\varphi_{i+1}) + \bar{y}_i cos(\varphi_i) - \bar{y}_{i+1} cos(\varphi_{i+1}), && (15)
\end{aligned}$$

where $i \in \{9, 10\}$ for the elbow and the wrist joints. The constraints link together the centres of gravity of all neighbouring couples of segments. So the whole system has $3n - m = 33 - 20 = 13$ degrees of freedom that are the initial position and rotation of the base body and 10 further relative rotations of the open-tree linked system of rigid bodies. The system of equations is conservative and the kinetic and the potential energies have the forms

$$\begin{aligned}
E_k &= \frac{1}{2}\sum_{i=1}^{n} m_i \left(\dot{x_i}^2 + \dot{y_i}^2\right) + \frac{1}{2}\sum_{i=1}^{n} I_i \dot{\varphi_i}^2, && (16)\\
E_p &= g\sum_{i=1}^{n} m_i y_i + \frac{1}{2}\sum_{(i,j)} k_{ij}\left(\varphi_{ij}\right)\varphi_{ij}^2, && (17)
\end{aligned}$$

where the limits (i, j) in the second term of the potential energy mean all segment couples connected by joints, k_{ij} is the particular relative rotation dependent joint rotational stiffnes and $\varphi_{ij} = \varphi_j - \varphi_i$ is the relative rotation of the two neighbouring segments. Considering the Lagrange's equations with multipliers have the form

$$\frac{\mathrm{d}}{\mathrm{d}t}\left(\frac{\partial L}{\partial \dot{q}_i}\right) - \frac{\partial L}{\partial q_i} = \sum_{j=1}^{m} \lambda_j \frac{\partial f_j}{\partial q_i}, \quad i \in \{1, \ldots, 3n\} \tag{18}$$

with the Lagrange's function $L = E_k - E_p$, we have the equations of motion in the form

$$\frac{\mathrm{d}}{\mathrm{d}t}\left(\frac{\partial E_k}{\partial \dot{q}_i}\right) + \frac{\partial E_p}{\partial q_i} = \sum_{j=1}^{m} \lambda_j \frac{\partial f_j}{\partial q_i} \quad i \in \{1, \ldots, 3n\}\,. \tag{19}$$

Equations (18) can be rewritten using the matrix notation as

$$\begin{bmatrix} \boldsymbol{M} & \boldsymbol{\Phi}_q^T \\ \boldsymbol{\Phi}_q & \boldsymbol{O} \end{bmatrix} \begin{bmatrix} \ddot{\boldsymbol{q}} \\ -\boldsymbol{\lambda} \end{bmatrix} = \begin{bmatrix} \boldsymbol{r} \\ \boldsymbol{\gamma} \end{bmatrix}, \tag{20}$$

where $\boldsymbol{M}$ is the mass matrix, $\boldsymbol{\Phi}_q$ is the matrix of constraint derivatives, $\boldsymbol{O}$ is the corresponding zero matrix, $\boldsymbol{r}$ is the external load matrix and $\boldsymbol{\gamma}$ is the matrix consisting of the rest after the constraint derivatives.

3.5. Contact definition

The model is defined by a linked open-tree multi-body system skeleton carrying the mass. For the purposes of pedestrian impact analysis, the contact forces play an important load. The contact forces express loading caused by the vehicle impact to the pedestrian. In order to model the contact well, each body of the multi-body system has to accommodate an external shape of the particular body segment. An ellipse attached to each segment is a good estimation for our purpose. Each segment ellipse is located by its centre to the segment centre (that is not necessarily its centre of gravity) and it is described by 2 semi-axes a_i and b_i as shown in Fig. 3. The scaling of the segment depth in the direction of the second semi-axis can be simply computed as $\bar{b}_i = k_i b_i$. The vehicle model is based on the approximation by rigid open polygon describing major vehicle frontal parts (bumper, bonnet and windshield) [10].

3.5.1. Collision detection

The shape of each segment Ω_i, $i \in \{1, \ldots, n\}$ is geometrically defined by an ellipse. Considering homogeneous coordinates $\boldsymbol{X} = [x, y, w]^T$, the ellipse can be written in the form

$$\boldsymbol{X}^T \boldsymbol{A} \boldsymbol{X} = 0\,. \tag{21}$$

Any ellipse with the semi-axes a_i and b_i parallel to the global coordinate system axes has the matrix in the form

$$\bar{\boldsymbol{A}}_i = \begin{bmatrix} \frac{1}{a_i^2} & 0 & 0 \\ 0 & \frac{1}{b_i^2} & 0 \\ 0 & 0 & -1 \end{bmatrix} \quad i \in \{1, \ldots, 11\}\,. \tag{22}$$

The segments of the human body models are positioned and angled in the plane by their generalized coordinates $[x_i, y_i, \varphi_i]^T$, $i \in \{1, \ldots, n\}$ that can define transformation matrix $\boldsymbol{R}_i$, $i \in \{1, \ldots, 11\}$ that transforms (rotates and moves) the basic ellipse (22) to the particular position defined by $[x_i, y_i, \varphi_i]^T$ in the plane. Such positioned ellipse can be written in the form

$$\boldsymbol{A}_i = \boldsymbol{R}_i^T \bar{\boldsymbol{A}}_i \boldsymbol{R}_i, \quad i \in \{1, \ldots, n\}\,. \tag{23}$$

The vehicle model is composed of s straight lines. Any segment Ω_i, $i \in \{1, \ldots, n\}$ defined geometrically by the particular ellipse defined by (23) can come into collision with one or more lines from the open polygon

$$\boldsymbol{X} = \boldsymbol{P}_l + (\boldsymbol{Q}_l - \boldsymbol{P}_l)t\,, \quad l \in \{1, \ldots, s\}\,, \quad t \in [0, 1] \tag{24}$$

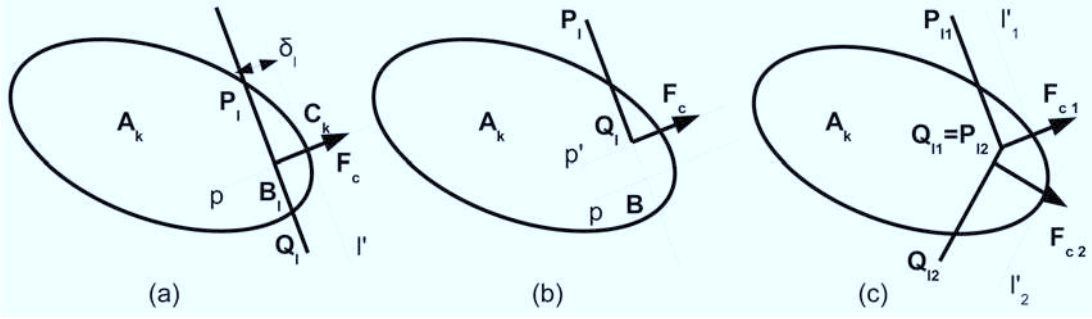

Fig. 4. Collision detection with contact force identification

that leads to a quadratic equation. Negative discriminant means no collision, zero or positive discriminant means contact or penetration.

Talking about contacts in multi-body dynamics, the energy absorption must be implemented in the internal contact variables since the rigidity of the contacting bodies. Furthermore, correct contact modelling in multi-body approach to biomechanics is crucial due to the high deformation of biological materials. Based on literature review, the continuous contact model, also referred to as compliant contact model, is chosen [5]. The basis of the continuous contact model is to measure the penetration of the contacting bodies, see Fig. 4a. This is done by defining the normal contact force F_n as an explicit function of local penetration δ and its rate as

$$F_n = F_n\left(\delta, \dot{\delta}\right). \tag{25}$$

For the total contact force, the simplified nonlinear spring-dashpot contact force model including tangential friction is used in the current paper as

$$\boldsymbol{F}_c = \left[F_n\left(\delta\right) - b\dot{\delta}\right]\left(\boldsymbol{n} - f\boldsymbol{t}\right), \tag{26}$$

where $\boldsymbol{n}$ and $\boldsymbol{t}$ are the penetration normal and tangent vectors respectively, f is the friction coefficient. The force on penetration dependance for various vehicle parts is take from [10]. The penetratration depth is checked couple by couple (segment k to open polygon line l, see Fig. 4c over the whole human body and over the whole open polygon and the particular penetration depth is computed as the distance between the vehicle structure open polygon line l and the parallel line tangent to the ellipse surface l'. Mathematically the line parallel to the open polygon line is constructed as the general line l' tangent to the ellipse with the tangent vector $|\boldsymbol{P}_l\boldsymbol{Q}_l|$. There are 2 solutions for such task, so it is necessary to choose the solution l' that is closer to the line $|\boldsymbol{P}_l\boldsymbol{Q}_l|$ otherwise the situation appeared on the ellipse opposite side. Introducing the line l', the contact point $\boldsymbol{C}_k$ is also detected. The contact force point of action (here line of action since all forces of the same value applied on a line to a rigid body have the same action) is the intersection of the vehicle structure open polygon line l and the perpendicular line going through the tangent point of contact p. Let us denote the intersection between lines p and l as the bottom point $\boldsymbol{B}_l$. The force action line is constructed as the line p perpendicular to the line $|\boldsymbol{P}_l\boldsymbol{Q}_l|$ going through the contact point $\boldsymbol{C}_k$.

In several cases, an edge contact might happen, see Fig. 4b. If there is the edge contact (see Fig. 4b and Fig. 4c) and the bottom point $\boldsymbol{B}_l$ is introduced outside the open polygon line (t fall outside the interval $[0, 1]$, see Fig. 4b), the bottom point comes to the edge point $\boldsymbol{Q}_l$ where the penetration is currently highest. The force action line becomes then p'.

If the segment k is in contact with more open polygon lines (e.g. l_1 and l_2, see Fig. 4c), all contacts are treated separately and separate contact forces $\boldsymbol{F}_{c1}$ and $\boldsymbol{F}_{c2}$ act on the particular segment. There is no reaction on the vehicle considering its higher mass. Concerning the particular segment k, the forces $\boldsymbol{F}_{ci}$, $i \in \{1, \ldots, s\}$ are translated to its centre of gravity including a moment caused by translation. The contact forces acting from the $i \in \{1, \ldots, s\}$ contact pairs on segment k is decomposed to the global coordinate system axis and togehter with the moment appears then in the right hand side vector $\boldsymbol{r}$ in (20) as

$$\boldsymbol{r} = \begin{bmatrix} \vdots \\ \sum_{i=1}^{l} \boldsymbol{F}_{c_{kl}} \boldsymbol{e}_1 \\ \vdots \\ m_k g + \sum_{i=1}^{l} \boldsymbol{F}_{c_{kl}} \boldsymbol{e}_2 \\ \vdots \\ \sum_{i=1}^{l} \mathbf{M}_{kl} \\ \vdots \end{bmatrix} . \tag{27}$$

4. Results

Numerically, the complete simulation model is implemented and solved in the form

$$\begin{bmatrix} \boldsymbol{M} & \boldsymbol{\Phi}_q^T \\ \boldsymbol{\Phi}_q & \boldsymbol{O} \end{bmatrix} \begin{bmatrix} \ddot{\boldsymbol{q}} \\ -\boldsymbol{\lambda} \end{bmatrix} = \begin{bmatrix} \boldsymbol{r} \\ \boldsymbol{\gamma} \end{bmatrix} \tag{28}$$

that leads to the system of 33 second order non-linear ordinary differential equations

$$\ddot{\boldsymbol{q}} = \boldsymbol{M}^{-1} \left[\boldsymbol{r} + \boldsymbol{\Phi}_q^T \left(\boldsymbol{\Phi}_q \boldsymbol{M}^{-1} \boldsymbol{\Phi}_q^T \right)^{-1} \left(\boldsymbol{\gamma} - \boldsymbol{\Phi}_q \boldsymbol{M}^{-1} \boldsymbol{r} \right) \right] , \tag{29}$$

where $\boldsymbol{r}$ is the right hand side including also the first order derivative expressions. The Baumgart's stabilization [6] for better convergence is used to stabilize the system. It leads to the final form of the solution as

$$\ddot{\boldsymbol{q}} = \boldsymbol{M}^{-1} \left[\boldsymbol{r} + \boldsymbol{\Phi}_q^T \left(\boldsymbol{\Phi}_q \boldsymbol{M}^{-1} \boldsymbol{\Phi}_q^T \right)^{-1} \left(\boldsymbol{\gamma} - \alpha \dot{\Phi} - \beta^2 \Phi - \boldsymbol{\Phi}_q \boldsymbol{M}^{-1} \boldsymbol{r} \right) \right] , \tag{30}$$

where α and β are the Baumgart's stabilization constants. The system is numerically solved in MATLAB R2010a [11] computational environment using especially the *ode45* function for numerical integration and the *fzero* function for the contact point detection. Other mathematical operations concern standard matrix manipulation.

Fig. 5 shows a typical pedestrian kinematic state of the impact situation at time 75 ms after the impact in the developed software [9]. The impact takes into account a 5 %-tile female pedestrian impacted by the standard passengers' car defined by Kerrigan [10] with car initial velocity 30 km/h. Fig. 6 shows the head output, namely relative head to car position in plane, head velocity and head acceleration. The same output is stated in Fig. 7 for thorax. The accelerations are filtered by the Channel Frequency Class (CFC) [3]. In accordance with SAE J211,

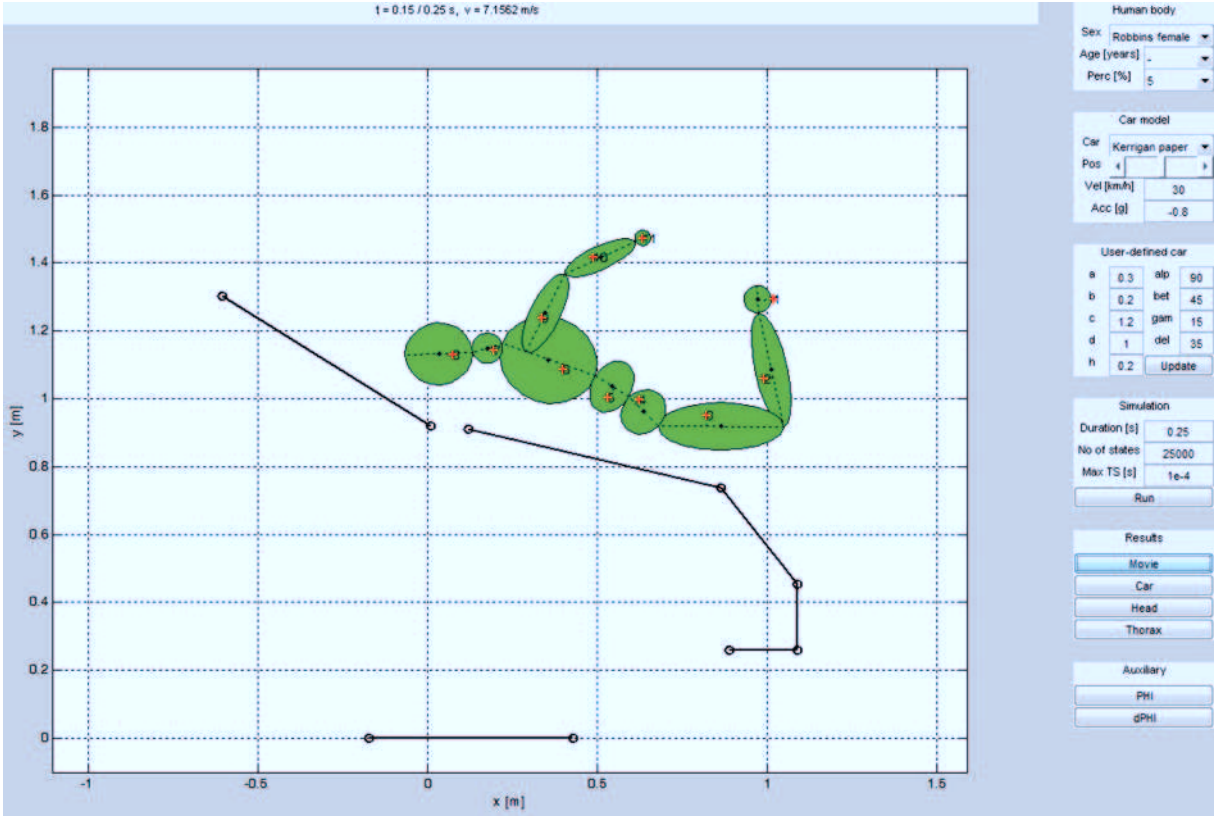

Fig. 5. Kinematic state

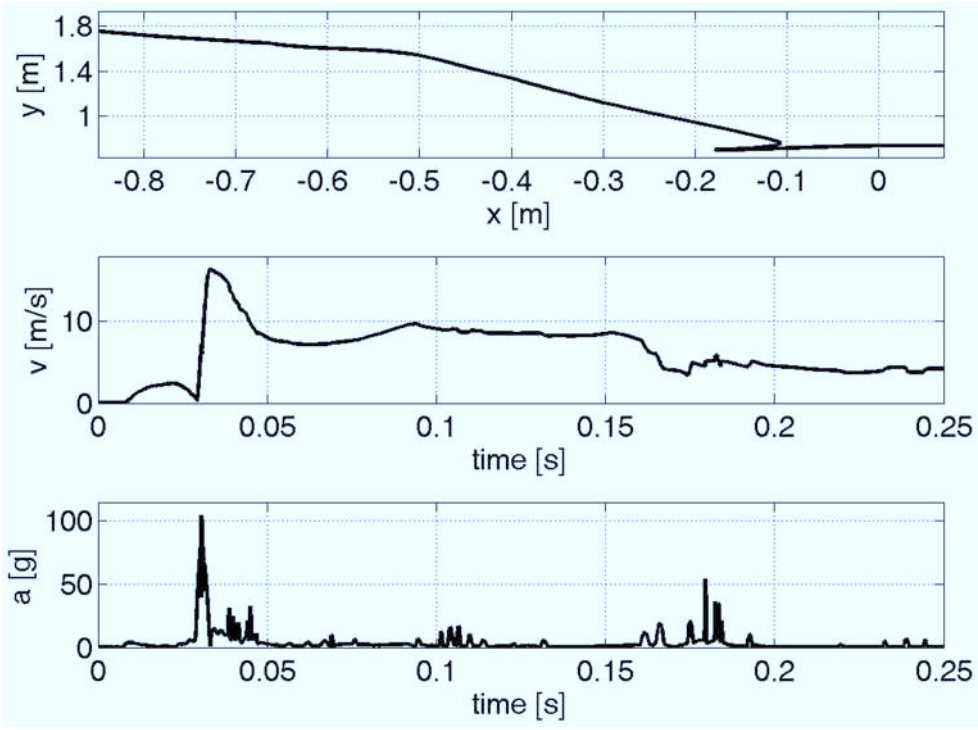

Fig. 6. Head output

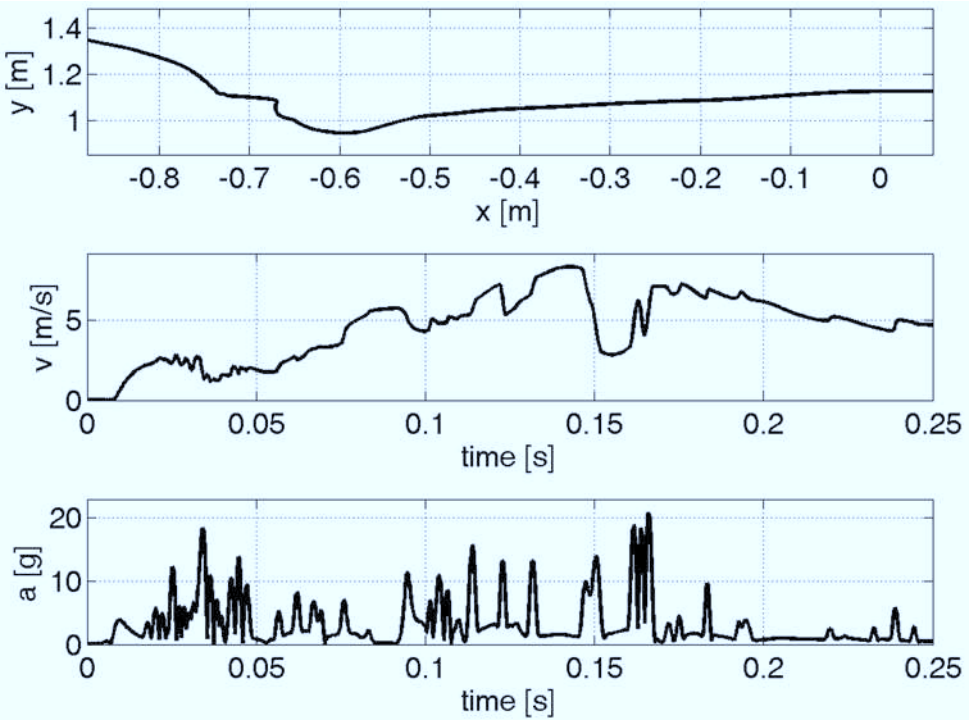

Fig. 7. Thorax output

a 4-channel Butterworth low pass filter with linear phase and special starting condition is used as a digital filter as

$$Y_i = a_0 X_i + a_1 X_{i-1} + a_2 X_{i-2} + b_1 Y_{i-1} + b_2 Y_{i-1}\,, \quad i \in 1, \ldots, N, \tag{31}$$

where X is the input signal, N is the number of samples and Y is the output filtered signal. The filter constants are calculated as [3]:

$$\begin{array}{lllllllll} \omega_d & = & 2\pi \cdot CFC \cdot 2.0775, & & a_0 & = & \frac{\omega_a^2}{1+\sqrt{2}\omega_a+\omega_a^2}, & & b_1 & = & \frac{-2(\omega_a^2-1)}{1+\sqrt{2}\omega_a+\omega_a^2}, \\ \omega_a & = & \frac{\sin\frac{T\omega_d}{2}}{\cos\frac{T\omega_d}{2}}, & & a_1 & = & 2a_0, & & b_2 & = & \frac{-1+\sqrt{2}\omega_a-\omega_a^2}{1+\sqrt{2}\omega_a+\omega_a^2}, \\ & & & & a_2 & = & a_0, & & & & \end{array} \tag{32}$$

where CFC is the filter parameter (180 for the thorax according to ISO 6487 and 1000 for the head according to SAE J211 [3]) and T is the sampling rate, here it is the time interval between 2 followed saved time history states. The difference equation describes a 2-channel filter. To realize a 4-channel filter, the data of the 2-channel filter has to run twice; once forwards and once backwards, to prevent phase displacements. The filter constants ω_d are calculated in the ISO 6487 sample code differently to SAE J211 as

$$\omega_d = 2\pi CFC \cdot 1.25 \cdot \frac{5}{3} = 2\pi \cdot CFC \cdot 2.08\overline{3}\,. \tag{33}$$

The current simulation results in $HIC = 25846$ that is really high considering fatal head injuries but typical for such simulation and in $3ms = 56$ that is under the injury limit [13].

4.1. Injury description

Injury criteria meassures related to the acceleration of the particular segment are implemented in order to analyze the particular injury of a human body [13]. Currently it concerns the head

injury criterion (*HIC*) and thethorax injury criterion (*3ms*). Whilst the $3ms$ criterion is the highest thorax acceleration lasting at least 3 miliseconds, the head injury criterion is stated as the integral

$$HIC = \max_{0 \le t_1 \le t_2 \le T} \left(\frac{1}{t_2 - t_1} \int_{t_1}^{t_2} a_{head}(t) dt \right)^{2.5} (t_2 - t_1), \tag{34}$$

where $a_{head}(t)$ is the head centre of gravity acceleration during the loading, t_2 and t_1 are two arbitrary times during the acceleration pulse. Time values are to be provided in seconds. For example, the victim of an accident sustains a head injury if $\mathrm{HIC}_{36} < 1\,000$, where the time window is $t_2 - t_1 \le 36$ ms.

5. Discussion

The above-mentioned study employs the standard multi-body system modelling approach for the used in biomechanics, especially the impact biomechanics. The main advantage of the multi-body system approach is the computation speed. The pedestrian impact scenario takes usually considerable time comparing to the standards crash simulation since the global kinematics of the pedestrian due to the free space after the impact. Hence the fast computation of the global kinematics including basic injury description is profitable. Such simulation can be followed by a deeper injury analysis e.g. by detailed finite element models whose have much higher requirements on computational time. Moreover, merging the multi-body system approach with some deformable elements like flexible joints, continuous contact models or even finite element parts ensure even wider exploitation of the model in the field of safety system development. The current study shows the planar approach that can be simply extended to the full 3D spatial modelling. The multi-body skeleton of the model can also carry realistic human shapes modelled by finite elements surfaces.

6. Conclusion

The paper shows a multi-body approach towards modelling of the human body response caused by the external impact loading. The human body is segmented into 11 major parts that compose together an open-tree linked multi-body structure. Particular neighbouring segments are connected by rotatinal joints with non-linear stiffness. Each segment carries a mass and inertial properties and its shape is simplified by an ellipse in order to simulate a contact surface. Continuous contact model based on penetration dependent contact force for each penetrating segment couples is implemented in order to asure correct impact loading due to the external contact. Age scaling concerning anthropometry, mass distribution and joint flexibility is derived. Injury criteria meassures are implemented in order to analyze the particular injury of a human body. The model serves for fast analysis of a frontal pedestrian impact that might go before a detailed analysis using more complex virtual human body models or physical tests with dummies. The 2D approach seems to be a promising fast tool for simple analysis even including multiple body contact.

Acknowledgements

The work is supported by the project CG911-044-150 of the Czech Ministry of Transport.

References

[1] Araújo, C. G., Flexibility assessment: normative values for flexitest from 5 to 91 years of age. Arq. Bras. Cardiol., 90 (2008) 257–263.

[2] Bláha, P., et al., Anthropometry of the Czechoslovak population from 6 till 55 years, Czechoslovak spartakiade. 1985 (in Czech).

[3] Cichos, D., de Vogel, D., Otto, M., Schaar, O., Zölsch, S., Crash Analysis Criteria Description. 2006.

[4] Daňková, A., Economical aspect of traffic accidents. Traffic engineering, 2007 (in Czech).

[5] Gilardi, G., Sharf, I., Literature survey of contact dynamics modelling. Mechanism and Machine Theory, 37 (2002) 1 213–1 239.

[6] Hajžman, M., Polach, P., Application of stabilization techniques in the dynamic analysis of multi-body systems. Applied and Computational Mechanics, 1 (2007) 479–488.

[7] Haug, E., Choi, H. Y., Robin, S., Beaugonin, M., Human models for Crash and impact simulation. Elsevier, North Holland, 2004.

[8] Hynčík, L., Nováček, V., Bláha, P., Chvojka, O., Krejčí, P., On scaling of human body models. Applied and Computational Mechanics, 1 (2007) 63–76.

[9] Hynčík, L., Čechová, H., Antroped2D: Software for 2d car to pedestrian frontal impact analysis.

[10] Kerrigan, J. R., Murphy, D. B., Drinkwater, D. C., Kam, C. Y., Bose, D., Crandall, J. R., Kinematic corridors for pmhs tested in full-scale pedestrian impact. University of Virginia Center for Applied Boimechanics, 2005.

[11] MathWorks, MATLAB R2010a.

[12] Robbins, D. H., Anthropometry of motor vehicle occupants. Technical report, 1983.

[13] Schmitt, K. U., Niederer, P., Walz, F., Trauma biomechanics, Introduction to accidental injury. Springer-Verlag, 2004.

[14] Skácal, L., Deep analysis of international comparison of traffic accidents in the Czech Republic. Transport Research Centre Brno, 2007 (in Czech).

[15] Czech Statistical Office, External death causes in the Czech Republic in years from 1994 till 2006 (in Czech).